RSC Advances

ROYAL SOCIETY OF CHEMISTRY

www.rsc.org/advances

Journal Name

ARTICLE

Highly sensitive mixed-potential type ethanol sensors based on stabilized zirconia and $ZnNb_2O_6$ sensing electrode

Received 00th January 20xx,
Accepted 00th January 20xx

DOI: 10.1039/x0xx00000x

www.rsc.org/

Fangmeng Liu, Xue Yang, Zhangduo Yu, Bin Wang, Yehui Guan, Xishuang Liang,* Peng Sun, Fengmin Liu, Yuan Gao and Geyu Lu*

The mixed-potential type stabilized zirconia (YSZ)-based gas sensor using columbite type composite oxide sensing electrode was developed and fabricated, aiming at sensitive detection of ethanol. Among the different oxide sensing electrodes (SEs) developed, the sensor attached with $ZnNb_2O_6$-SE was found to achieve the largest sensitivity to ethanol at 625°C. Furthermore, the result of the effect of sintering temperature on sensing characteristic showed that the sensor utilizing $ZnNb_2O_6$-SE sintered at 1000°C displayed the highest response of -175 mV to 100ppm ethanol and the low detection limit of 0.5ppm at 625°C. ΔV of the present sensor exhibited segmentally linear relationship to the logarithm of ethanol concentration in the ranges of 0.5–5 ppm and 5–200 ppm, which the sensitivities were -29 and -112mV/decade, respectively. Moreover, the fabricated device also displayed fast response and recovery times, good repeatability, small fluctuation during 30 days continuous high temperature of 625 °C measured periods, and acceptable selectivity to some other interfering gases. Additionally, the sensing mechanism involving mixed potential was further demonstrated by polarization curves.

1. Introduction

Ethanol processes flammable, volatile characteristics and much lower toxicity and harm to human health. However, ethanol detection has been strongly required in many fields, such as drink driving, breath marker for specific diseases, the control of fermentation processes.[1,2] Under laboratory conditions, ethanol can conventionally be detected using techniques such as IR, mass spectrometry, or gas chromatography.[3,4] Although these methods exhibit the advantage in terms of accuracy, selectivity, and detection of very low concentration. Obviously, their application is limited by cost, instrumentation complexity and vast size of instrumentation. Thus, for low-cost, compact and portable application, the gas sensor has attracted considerable attention for real-time detection of ethanol.

Among various gas sensors, mixed-potential type solid-state electrochemical gas sensors utilizing yttria-stabilized zirconia (YSZ) solid electrolyte and metal oxide sensing electrode (SE) has been developed extensively for the past two decades, and are widely applied for high performance gas sensing detection, such as NO_x, H_2, CO, NH_3 and VOCs.[5-19] The working principle of such sensors is related to mixed-potential mechanism and has been described in details by several research groups.[10-22] For mixed-potential type gas sensor, the sensing signal (V) is generated at sensing electrode due to the simultaneous occurrence of the electrochemical reactions involving oxygen and target gas. Thus, the selection of a suitable SE material is one of the most important points to achieve high sensing performance.

In this work, various columbite type composite oxide materials ($ZnNb_2O_6$, $NiNb_2O_6$ and $CoNb_2O_6$) were developed via a facile sol-gel method. For the first time, three kinds of oxide-SEs were used to fabricate the planar mixed-potential type YSZ-based gas sensors for sensitive detection of ethanol and the corresponding sensing performances were examined. Among oxide-SEs developed, the sensor attached with $ZnNb_2O_6$-SE gave the highest sensitivity to ethanol at 625 °C. The effect of sintering temperature of $ZnNb_2O_6$-SE on sensing property was studied. Additionally, the gas sensing characteristics of the present device to ethanol were systematically investigated and the sensing mechanism was also discussed.

2. Experimental

2.1 Preparation and characterization of columbite type sensing electrode material

The $ZnNb_2O_6$ was synthesized via a sol-gel method from Zinc nitrate hexahydrate ($Zn(NO_3)_2{\cdot}6H_2O$), Niobium oxide (Nb_2O_5), HF acid (40%), Ammonium hydroxide ($NH_3{\cdot}H_2O$), Citric acid (CA), and Ammonium nitrate (NH_4NO_3). All of reagents were of analytical grade without further purification and provided by Sinopharm Corp., China. In a typical synthesis process, 3mmol Nb_2O_5 was dissolved in a certain amount of HF acid after heating in water bath of 80°C. Then, ammonia hydroxide solution was dropwise added to the above solution until the PH value was up to 9 to obtain $Nb_2O_5{\cdot}nH_2O$ precipitate under stirring constantly. The precipitate was filtered,

State Key Laboratory on Integrated Optoelectronics, College of Electronic Science and Engineering, Jilin University, 2699 Qianjin Street, Changchun 130012, China E-mail: liangxs@jlu.edu.cn; lugy@jlu.edu.cn; Fax: +86-431-85167808; Tel: +86-431-85167808

washed, and dissolved in citric acid aqueous solution and stirred at 80 °C for 2h. Then, the stoichiometric $Zn(NO_3)_2{\cdot}6H_2O$ and NH_4NO_3 (the molar ratio of $Zn/Nb/NH_4NO_3$=1:2:12) were added into the solution described above and then stirred at 80 °C until to a gel was obtained. The resultant gel was maintained at 80 °C for 24 h at vacuum drying oven. The MNb_2O_6 (M: Co and Ni) materials were prepared by the same method according to the procedure described above. The precursor gel was then introduced into a muffle furnace and sintered at 1000 °C for 2 h to get target products, respectively. Additionally, in order to investigate the effect of sintering temperature on sensing performance, $ZnNb_2O_6$ was sintered at 800, 1000 and 1200°C for 2 h, respectively.

The structural properties of the products were characterized with Rigaku wide- angle X-ray diffractometer (D/max rA, using Cu Kα radiation at wave length =0.1541 nm) in the angular range of 20–80° . Field-emission scanning electron microscopy (FESEM) measurements of surface morphology of the $ZnNb_2O_6$-SE materials were performed using a JEOL JSM-7500F microscope with an accelerating voltage of 15 kV.

2.2 Fabrication and measurement of gas sensor

The sensor was fabricated using the YSZ plate (8 mol% Y_2O_3-doped, 2 mm×2 mm square, 0.3 mm thickness, provided by Anpeisheng Corp., China). A point-shaped and a narrow stripe-shaped Pt electrode (reference electrode, RE) were formed on two ends of the YSZ plate using a commercial Pt paste (Sino-platinum Metals Co., Ltd.), and sintered at 1000 °C. The various sensing electrode materials were mixed with a minimum quantity of deionized water to obtain required pastes, respectively. Then, the resultant paste was applied on the point-shaped Pt to form stripe-shaped sensing electrode (SE), and then the device was sintered at 800 °C for 2h to gain good contact between the sensing electrode and electrolyte. The Pt heater printed on Al_2O_3 substrate was then fixed to the YSZ plate by the inorganic adhesive, which provided the required heating temperature for the sensor. The schematic diagram of the fabricated sensor is shown in Fig. 1.

The gas sensing characteristics of the fabricated sensors were measured by a conventional static method.[23,24] The electric potential difference (V) between the SE and the RE was measured with a digital electrometer (Rigol Technologies, Inc., DM3054, China)

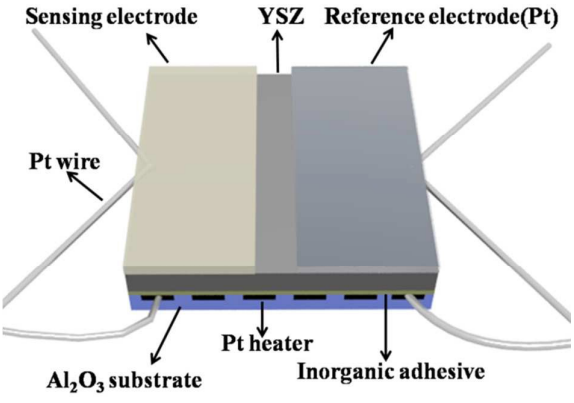

Fig. 1 Schematic diagram of fabricated sensor.

when the sensor was exposed to air or sample gas. The results obtained were recorded with a computer connected to the electrometer. The desired concentration of sample gas was obtained by the static liquid gas distribution method, which was calculated by the following formula.[25,26]

$$C = \frac{22.4 \times \rho \times \varphi \times V_1}{M \times V_2} \times 1000$$

Where, C (ppm) is the required target gas concentration; ρ (g/mL) the density of the liquid; φ the required gas volume fraction; V_1 (μL) and V_2 (L) the volume of the liquid and chamber, respectively; and M (g/mol) the molecular weight of the liquid. The current–voltage (polarization) curves of the sensor were carried out via the potentiodynamic method (CHI625C, Instrument corporation of Shanghai, China) using a two-electrode configuration in the base gas (air) and the different concentrations of ethanol gas (50, 100, and 200ppm) at 625 °C.

3. Results and discussion

The typical XRD patterns of $ZnNb_2O_6$ composite oxide materials annealed at different temperatures are presented in Fig. 2. The sharp diffraction features suggest the good crystalline nature of the prepared $ZnNb_2O_6$ composite oxide sensing electrode materials. The diffraction peaks in the pattern of $ZnNb_2O_6$ sintered at 800, 1000 and 1200 °C can be readily indexed to columbite type structure of $ZnNb_2O_6$ (JCPDS#76-1827).[27-29] No characteristic peaks from impurities in $ZnNb_2O_6$ samples are detected. The morphologies of $ZnNb_2O_6$-SE sintered at different temperatures (800, 1000, and 1200 °C) were studied by FESEM and results are shown in Fig. 3. Obviously, as shown in Fig. 3(a-c), the porous structure was observed and such structure contributed to diffusion of the gas molecular within the material. Additionally, the size of particle increased gradually with the increasing of sintering temperature. Fig. 3(d) displayed EDS mapping images of surface of $ZnNb_2O_6$-SE sintered at 1000 °C. For the single columbite phase $ZnNb_2O_6$, the elemental mapping measurement further confirms the coexistence

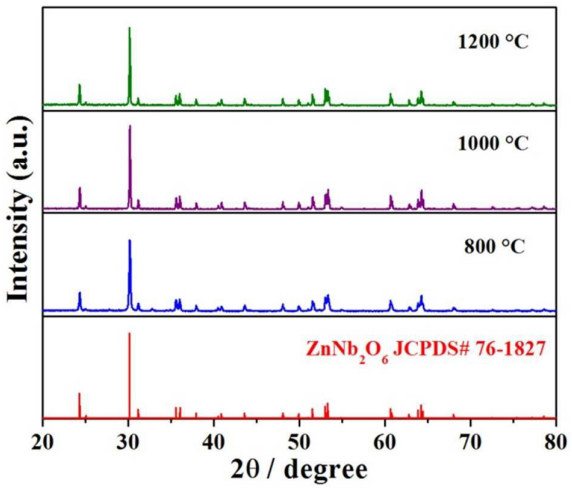

Fig. 2 XRD patterns of $ZnNb_2O_6$ composite oxide material sintered at 800, 1000 and 1200 °C.

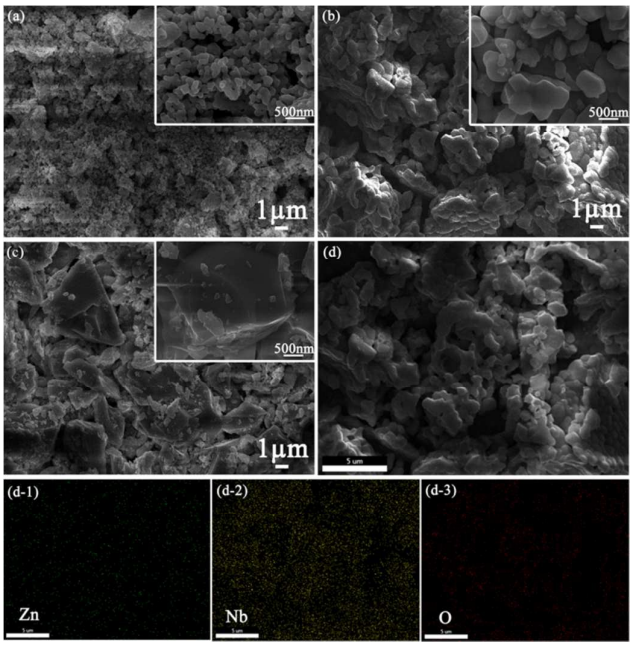

Fig. 3 SEM images of $ZnNb_2O_6$-SEs sintered at different temperatures: (a) 800 °C; (b) 1000 °C; (c) 1200 °C; (d) EDS mapping images for the element of Zn, Nb and O of $ZnNb_2O_6$ sintered at 1000 °C.

and homogeneous dispersion of Zn, Nb and O elements.

In order to find out the most suitable sensing electrode material, three kinds of columbite type oxides ($ZnNb_2O_6$, $NiNb_2O_6$ and $CoNb_2O_6$) were used to form the sensing electrode layer of YSZ-based sensors, and responses of fabricated devices to 100ppm ethanol were measured at 625°C. It is noteworthy that, as shown in Fig. 4(a), the sensor utilizing $ZnNb_2O_6$-SE was found to exhibit the highest response value to ethanol, comparing with devices attached with other oxide materials. Thus, the sensing properties of the sensor attached with $ZnNb_2O_6$-SE are investigated below at 625°C in more detail. For this kind of gas sensor, the sensing characteristic of sensor was affected by sintering temperature of sensing electrode material.[30-32] The sensors using $ZnNb_2O_6$-SE calcinated at 800 °C, 1000 °C and 1200 °C were fabricated and the responses to 100ppm ethanol for fabricated devices were displayed in Fig. 4(b). It is apparent that the sensor utilizing $ZnNb_2O_6$-SE annealed at 1000 °C exhibited the largest response values to ethanol in examined concentration comparing with the devices attached with $ZnNb_2O_6$-SE sintered at other temperatures. The sensing characteristics of

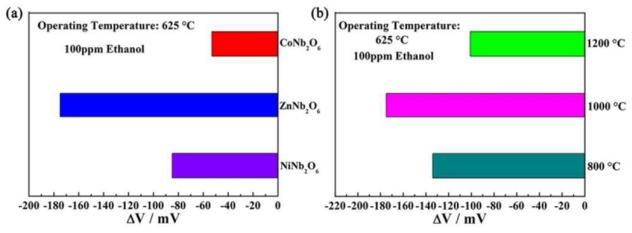

Fig. 4 (a) Response to 100ppm ethanol for sensors using different sensing electrodes; (b) Response to 100ppm of ethanol for sensors attached with $ZnNb_2O_6$-SE calcined at different temperatures.

present devices related to the mixed potential mechanism, the sensor can be presented as the following electrochemical cells:

In air: O_2, $ZnNb_2O_6$/YSZ/Pt, O_2

In sample gas: $C_2H_5OH + O_2$, $ZnNb_2O_6$/YSZ/Pt, $C_2H_5OH + O_2$

When the ethanol gas arrived at the TPB (triple phase boundary, the interface of $ZnNb_2O_6$-SE, ethanol and YSZ), the cathodic reaction of O_2 (1) and anodic reaction of ethanol (2) take place simultaneously at the TPB and form a local cell, as shown in Fig. 5. The rates of two electrochemical reactions are equal to each other, the dynamic equilibrium is reached, and the electrode potential is regarded as the mixed potential. The potential difference of the sensing electrode and reference electrode is expressed as the sensing signal.

Cathodic reaction: $O_2 + 4e^- \rightarrow 2O^{2-}$ (1)

Anodic reaction: $C_2H_5OH + 6O^{2-} \rightarrow 2CO_2 + 3H_2O + 12e^-$ (2)

For the present device, the sensing signal is strongly dependent on the ethanol concentration reached to TPB and degree of electrochemical reactions at TPB. Taking these factors into consideration, the porous structure of SE layer and higher electrochemical reaction to ethanol will achieve higher sensing performance. The porous channels decreased the consumption of ethanol in the process of diffusion in $ZnNb_2O_6$ electrode layer and facilitate more ethanol gas to reach the TPB, which participated directly in electrochemical reactions. However, the microstructure of $ZnNb_2O_6$ particle should be taken into account, the particles became too large with the further increase of annealing temperature and then the interface area of the enlarged particle and YSZ increased, but TPB area reduced and electrochemical reaction active sites decreased. In this case, the sensitivity of the sensor to ethanol decreased. As presented above, the crystallization of $ZnNb_2O_6$ increased with the increasing of sintering temperature, which affected the electrochemical activity. Therefore, both of the crystallization and microstructure of SE affect the response variation of sensor to ethanol. The excellent balance of the electrochemical activity and TPB length was formed when the annealed temperature is 1000°C and the highest response to ethanol was achieved. Thus, the sensor using $ZnNb_2O_6$ sintered at 1000 °C was paid considerable attentions to investigate in the following sections.

For further clarifying the reason for the highest response of the sensor utilizing $ZnNb_2O_6$-SE annealed at 1000 °C and validating the proposed mixed-potential mechanism, polarization curves of the sensor attached with MNb_2O_6 (M: Zn, Co, and Ni)-SE and $ZnNb_2O_6$ sintered at different temperatures in air and 100 ppm ethanol and polarization curves of the sensor utilizing $ZnNb_2O_6$-SE sintered at

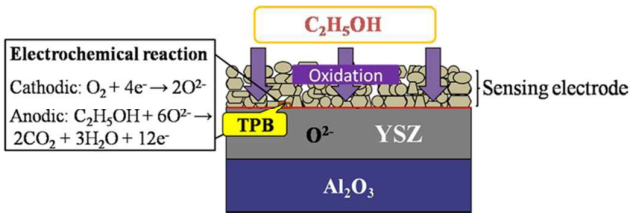

Fig. 5 Sensing model of fabricated sensor.

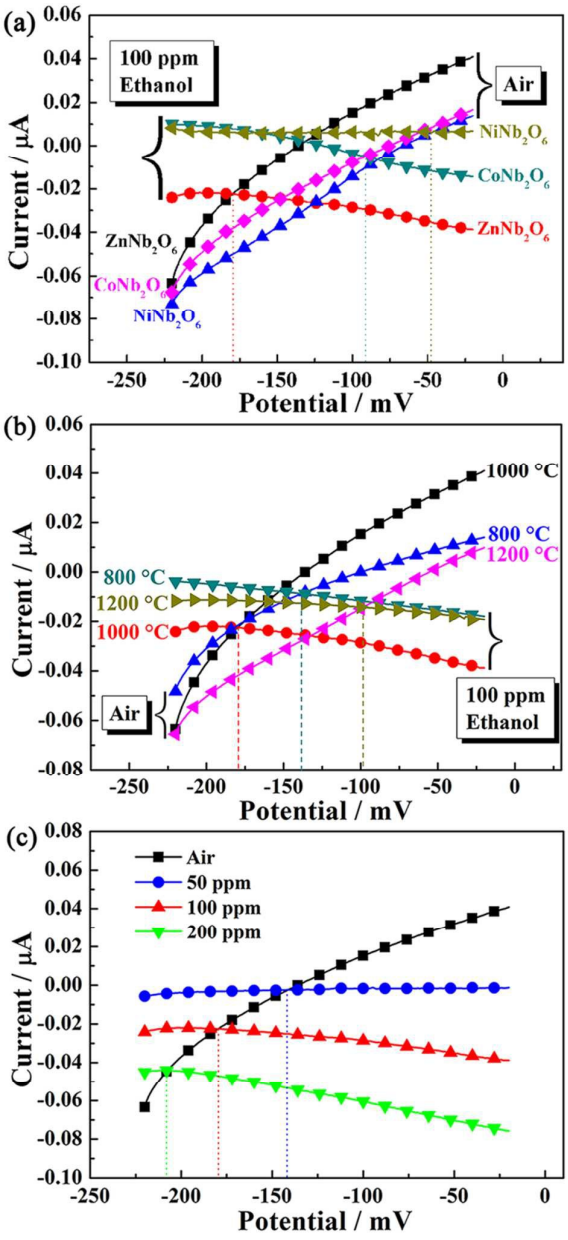

Fig. 6 (a) Polarization curves in air and 100 ppm ethanol for sensors using different sensing electrodes at 625 °C; (b) Polarization curves in air and 100 ppm ethanol for sensors attached with $ZnNb_2O_6$-SE sintered at different temperatures; (c) Polarization curves in different concentrations of ethanol for the sensor attached with $ZnNb_2O_6$-SE sintered at 1000 °C.

1000 °C in different concentrations of ethanol at 625 °C were measured and shown in Fig. 6.[33] The cathodic polarization curve was obtained in air, and the anodic polarization curve was obtained by subtracting in air from in sample gas (different concentration of ethanol + air). From Fig. 6(a), it can be clearly seen that the polarization curve for the anodic reaction of ethanol for the device using $ZnNb_2O_6$-SE shifts downward to higher current values, compared with that of other SEs. This shift of polarization curve is considered to the electrochemical reaction of ethanol. It was assumed that the shift of current at electrode potential was ascribed to the current due to anodic reaction (2) of ethanol. This indicates that sensor attached with $ZnNb_2O_6$-SE exhibits the highest electrochemical catalytic activity to anodic reaction (2) of ethanol. In this case, the sensor attached with $ZnNb_2O_6$-SE displayed the highest sensitivity to ethanol at 625 °C. Similarly, as shown in Fig. 6(b), the sensor attached with $ZnNb_2O_6$-SE sintered at 1000°C also displays the highest electrochemical catalytic activity to anodic reaction of ethanol, by comparing the anodic polarization curves of the sensors using $ZnNb_2O_6$-SE sintered at different temperatures. Additionally, the mixed potential can be estimated from the intersection of the cathodic and anodic polarization curves.[34,35] Based on the comparison of the mixed potential estimated values and the potential difference values experimentally observed for fabricated three sensors and the device utilizing $ZnNb_2O_6$-SE annealed at 1000 °C to different concentration of ethanol at 625 °C, in Table 1, the estimated values are in close proximity to those observed values. These coincidences supported the sensing mechanism involving the mixed potential.[36-39]

It is well known that the response of the sensor is strongly influenced by the operation temperature. In order to determine the optimal operating temperature of the sensor attached with $ZnNb_2O_6$-SE annealed at 1000 °C to ethanol, the responses of device fabricated to 50ppm ethanol at different operating temperatures were tested as a function and the results are presented in Fig. 7. It can be observed that the response to 50 ppm ethanol for fabricated sensor tended to increase and reached the highest response value at operating temperature of 625 °C, and then decreased with a further rise of operating temperature. The occurrence of the electrochemical reaction for the present device at TPB needed definite activation energy. The electrochemical reaction did not gain enough activation energy below 625 °C, thus, the sensitivity of the sensor to ethanol increased with the increasing of temperature. However, the desorption process of ethanol exhibited dominant above 625 °C, and the amount of ethanol reached the TPB became less and less along with the further increase of operating temperature. Namely, the response of the sensor to ethanol was reduced. Consequently, the optimal operating temperature for the present sensor was considered to be 625 °C.

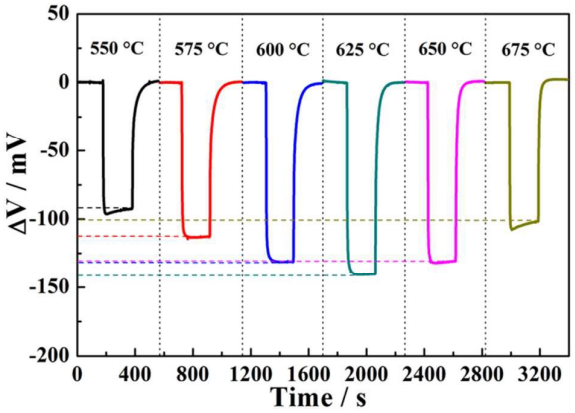

Fig. 7 Response and recovery transients for the sensor using $ZnNb_2O_6$-SE sintered at 1000°C to 50ppm ethanol at different operating temperatures.

Table 1 Comparison of the mixed potential estimated and the potential difference value observed for the sensors attached with $ZnNb_2O_6$-SEs sintered at different temperatures and device using $ZnNb_2O_6$-SE sintered at 1000°C to different concentration of ethanol.

Sensors	Ethanol Conc. (ppm)	Mixed potential (estimated) (mV)	Potential difference value (observed) (mV)
$ZnNb_2O_6$ (800 °C)–SE	100	-138.5	-134
$ZnNb_2O_6$ (1200 °C)–SE	100	-98	-101
$ZnNb_2O_6$ (1000 °C)–SE	100	-179	-175
$ZnNb_2O_6$ (1000 °C)–SE	50	-142	-141
$ZnNb_2O_6$ (1000 °C)–SE	200	-208	-205

Table 2 Comparison of the sensing performance of the present sensor and those of devices reported in literatures.

Material	Ethanol Conc. (ppm)	Response (mV)	Sensitivity (mV/decade)	Low detection limit (ppm)	Reference
$ZnNb_2O_6$	50	–141	–112	0.5 (5mV)	Present work
$Pt/MoO_3/SnO_2$	100	13	41	–	43
$Pt/CeO_2/SnO_2$	100	28	49	–	43
In_2O_3/SnO_2	100	53.2 ($R=R_a/R_g$)	–	–	2
CdO/ZnO	100	76 ($R=R_a/R_g$)	–	0.5 (1.3)	44
Cr_2O_3/ZnO	100	25 ($R=R_a/R_g$)	–	1 (3.6)	45
$In_{2-x}Ni_xO_3$	100	80 ($R=R_a/R_g$)	–	1 (5)	46
SnO_2/α-Fe_2O_3	100	16 ($R=R_a/R_g$)	–	10 (3)	47

The response transients of fabricated sensor attached with $ZnNb_2O_6$-SE annealed at 1000 °C toward different concentrations of ethanol in the range of 5–200 ppm was examined at 625 °C and the results obtained are shown in Fig. 8 (a). It is obvious that the sensor

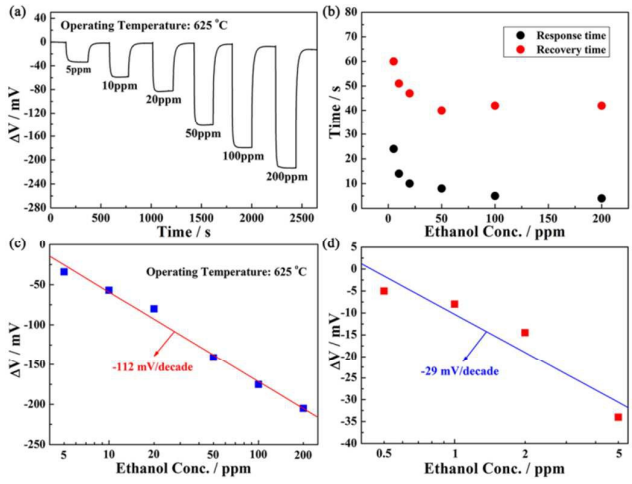

Fig. 8 (a) Response transients for the sensor attached with $ZnNb_2O_6$-SE sintered at 1000 °C toward different concentrations of ethanol in the range of 5–200ppm at 625 °C and (b) its corresponding response and recovery times; (c, d) Dependence of ΔV on the ethanol concentration at 625 °C for the sensor attached with $ZnNb_2O_6$-SE sintered at 1000 °C.

reached quickly steady state value when exposed to ethanol atmosphere, and the response increased with the increase of ethanol concentration. The response for the sensor attached with $ZnNb_2O_6$-SE annealed at 1000 °C to 5 and 200 ppm ethanol at 625°Cwas -34 and -205 mV, respectively. Besides, the response and recovery times of present sensor were also further evaluated according to Fig. 8 (a). As shown in Fig. 8 (b), the response and recovery process become shortened with increasing gas concentration, which may be attributed to the lower gas concentration requiring more time to reach equilibrium. The typical 90% response and recovery times of the present device toward 50ppm of ethanol are 8 and 40s, which exhibits fast response and recovery rates. Furthermore, the dependence of ΔV for the sensor attached with $ZnNb_2O_6$-SE sintered at 1000 °C on the ethanol concentration in the examined range at 625 °C is shown in Fig. 8 (c). In this case, almost linear relationships between the ΔV and the logarithm of ethanol concentration in range of 5–200 ppm at 625 °C were observed, which conforms to mixed potential type model. The sensitivity (slope) of present sensor is -112 mV/decade. Moreover, the present sensor even can detect 500ppb ethanol, which the response value is -5 mV. Clearly, the sensitivity to ethanol in the range of 0.5–5ppm for fabricated sensor is -29 mV/decade (Fig. 8 (d)). The reason for the occurrence of such a linear dependence of ethanol sensitivity is may be followed. As known very well, the electrochemical reaction for the present mixed potential type ethanol sensor occurred at the TPB. And the sensing signal of the sensor depended on the concentration of ethanol at TPB of

$ZnNb_2O_6$-SE and the amount of active sites of TPB. For the low concentration range of ethanol (0.5–5 ppm), the amount of TPB active sites for the present sensor are enough to provide the electrochemical reaction, thereby, the sensitivity of the sensor are mainly related to the amount of ethanol reached the TPB of $ZnNb_2O_6$-SE. Although with porous channels in sensing electrode layer, a certain amount of gas was still consumed in the process of diffusion. When the concentration of the measured ethanol is at a lower level, the ethanol consumption accounted for the proportion of the total quantity of ethanol is larger than that of higher ethanol concentration (5–500 ppm). Therefore, the relatively low sensitivity to ethanol concentration in the range of 0.5–5ppm was observed. Moreover, the continuous response-recovery and selectivity for gas sensor are important sensing performance parameters. The continuous response and recovery transients of the present sensor to 50 ppm ethanol at 625 °C, as illustrated in Fig. 9 (a). It is clearly seen that the responses of the present device to 50 ppm ethanol had little fluctuation and the best change error was -3.5% in the examined nine-time cycles, which indicated that the sensor displayed good repeatability. Fig. 9 (b) shows the cross-sensitivities for the sensor attached with $ZnNb_2O_6$-SE annealed at 1000 °C to various gases at 625 °C, such as toluene, benzene, acetone, methanol, NO_2 and NH_3, etc. It is obvious that the sensor present fabricated exhibited relative high responses to 50 and 100ppm of ethanol comparing with those of other interfering gases. But, the effect of the acetone and methanol as interfering gas on ethanol response for the fabricated sensor could not be ignored. As has

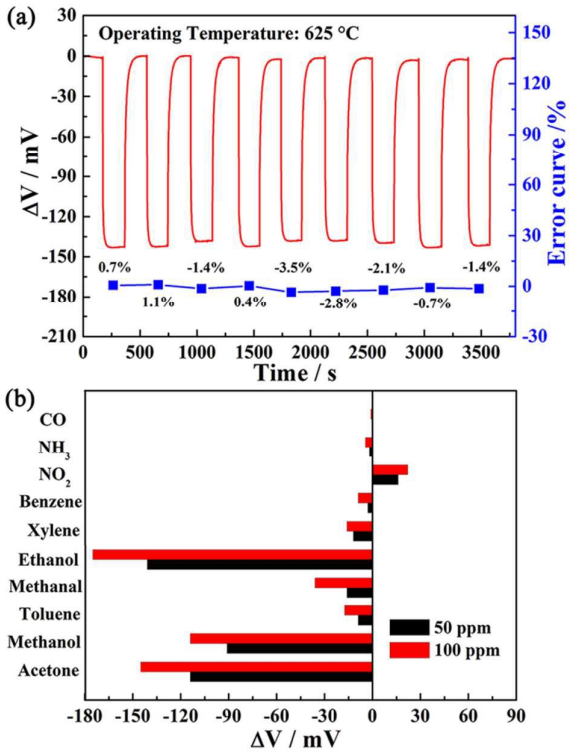

Fig. 9 (a) Continuous response and recovery transients of the sensor attached with $ZnNb_2O_6$-SE sintered at 1000°C to 50ppm ethanol at 625 °C; (b) Cross-sensitivities for the sensor attached with $ZnNb_2O_6$-SE sintered at 1000°C to various gases at 625 °C.

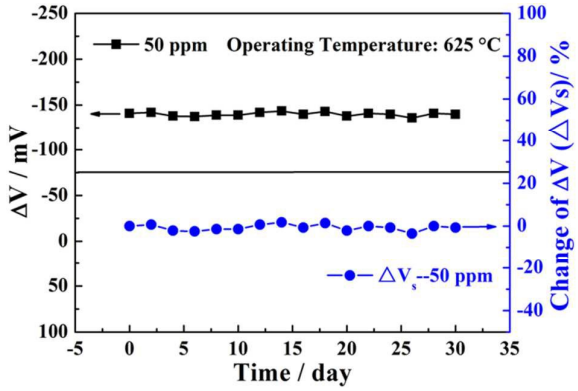

Fig. 10 Long-term stability to 50 ppm ethanol at 625 °C for the sensor attached with $ZnNb_2O_6$-SE sintered at 1000°C.

reported previously [40-42], these species is difficult to be selected using fabricated sensor. The reasons may be as follows: the identification of sensing electrode material is relative weak to identify similar kinds of chemical species (ethanol, acetone and methanol) or $ZnNb_2O_6$ sensing electrode material developed displayed the similar electrochemical catalytic reaction activity to ehtanol, acetone and methanol, which induce to a little difference in sensitivity. Thus, the present device is insufficient in selectivity of certain gases. Perhaps development of new sening electrode material with high electrochemical catalytic activity to certain signal gas, fabrication of array of sensor or change of device structure is good strategy. The improvement of selectivity to acetone and methanol remains to be further investigated in the future work. On the whole, however, the present sensor still displayed acceptable selectivity to most of various interfering gases.

For a point of view in actual application of the sensor, the sensitivity to a target gas should not be affected under the long-term working condition. The stability of the sensor present fabricated was investigated by continuous working at high temperature of 625 °C during interval of 30 days. The responses of the sensor to 50 ppm ethanol were measured every other day. And obtained results were depicted in Fig. 10. It can be seen that, from Fig. 10, the change amplitude of ΔV for the sensor attached with $ZnNb_2O_6$-SE sintered at 1000 °C varied slightly to 50 ppm ethanol during 30 days measurement period. In order to further illustrate exactly the change amplitude of ΔV with time, the change of ΔV (ΔV_s) for the sensor is given by $\Delta V_s = [(\Delta V_n - \Delta V_0)/ \Delta V_0 \times 100\%]$, where ΔV_n and ΔV_0 denote ΔV of the sensor on the n and initial day, respectively. The quantitative result showed that $\triangle V_s$ for the sensor to 50 ppm ethanol during the 30 day was less than 4%, which the sensor has good stability. Based on above results, the comparison of the ethanol sensing property for the fabricated sensor and that reported previously in literature is presented in Table 2. Obviously, the present device exhibited better sensing performance in terms of response, sensitivity and low detection limit to ethanol than previously reported devices.

4. Conclusions

In this paper, the compact solid-state electrochemical ethanol sensor based on YSZ and columbite type complex oxide sensing electrode synthesized via the facile sol-gel method was developed. Among the oxide SEs examined, $ZnNb_2O_6$ was found to be best suited for sensing electrode of YSZ-based ethanol device. The sensor attached with $ZnNb_2O_6$-SE sintered at 1000 °C displayed the highest response to ethanol at 625 °C. The present sensor showed the low detection limit of 500 ppb to ethanol, and ΔV of the device exhibited segmentally linear relationship to the logarithm of ethanol concentration in the ranges of 0.5–5 ppm and 5–200ppm, which the slope were -29 and -112 mV/decade. Furthermore, the present device also exhibited good repeatability, acceptable selectivity and excellent stability during measurement period of 30 days at high-temperature-aging of 625 °C. For above-mentioned sensing performance of mixed potential type sensor fabricated, the present sensor can be considered as a potential candidate in detecting ethanol.

Acknowledgements

This work is supported by the National Nature Science Foundation of China (Nos. 61134010, 61327804, 61374218, 61473132, 61533021, and 61520106003), Program for Chang Jiang Scholars and Innovative Research Team in University (No. IRT13018) and National High-Tech Research and Development Program of China (863 Program No. 2014AA06A505), Application and Basic Research of Jilin Province (2013010 2010JC).

Notes and references

1 A. Yazıcı, N. Dalbul, A. Altındal, B. Salih, Ö. Bekaroğlu, *Sens. Actuators, B,* 2014, **202**, 14–22.
2 Y. Liu, S. Yao, Q. Yang, P. Sun, Y. Gao, X. Liang, F. Liu, G. Lu, *RSC Adv.,* 2015, **5**, 52252–52258.
3 M. Shnayderman, B. Mansfield, P. Yip, H. Clark, M. Krebs, S. Cohen, J. Zeskind, E. Ryan, H. Dorkin, M. Callahan, T. Stair, J. Gelfand, C. Gill, B. Hitt, C. Davis, *Anal. Chem.,* 2005, **77**, 5930–5937.
4 M. Franke, T. Koplin, U. Simon, *Small*, 2006, **2**, 36–50.
5 N. Miura, H. Kurosawa, M. Hasei, G. Lu, N. Yamazoe, *Solid State Ionics*, 1996, **86-88**, 1069–1073.
6 G. Lu, Miura, N. Yamazoe, *J. Appl. Electrochem.*, 1998, **28**, 1009–1011.
7 G. Lu, Miura, N. Yamazoe, *Sens. Actuators, B,* 2000, **65**, 125–127.
8 Q. Diao, C. Yin, Y. Liu, J. Li, X. Gong, X. Liang, S. Yang, H. Chen, G Lu, *Sens. Actuators, B,* 2013, **180**, 90–95.
9 F. Liu, Y. Guan, M. Dai, H. Zhang, Y. Guan, R. Sun, X. Liang, P. Sun, F. Liu, G. Lu, *Sens. Actuators, B,* 2015, **216**, 121–127.
10 S. Anggraini, M. Breedon, N. Miura, *Sens. Actuators, B,* 2013, **187**, 58–64.
11 Y. Li, X. Li, Z. Tang, Z. Tang, J. Yu, J. Wang, *Sens. Actuators, B,* 2015, **206**, 176–180.
12 T. Hübert, L. Boon-Brett, G. Black, U. Banach, *Sens. Actuators, B,* 2011, **157**, 329–352.
13 N. Miura, T. Raisen, G. Lu, N. Yamazoe, *Sens. Actuators, B,* 1998, **47**, 84–91.
14 Y. Fujio, V. Plashnitsa, M. Breedon, N. Miura, *Langmuir*, 2012, **28**, 1638–1645.
15 F. Liu, R. Sun, Y. Guan, X. Cheng, H. Zhang, Y. Guan, X. Liang, P. Sun, G. Lu, *Sens. Actuators, B,* 2015, **210**, 795–802.
16 Y. Fujio, T. Sato, N. Miura, *Solid State Ionics*, 2014, **262**, 266–269.
17 Y. Suetsugu, T. Sato, M. Breedon, N. Miura, *Electrochim. Acta*, 2012, **73**, 118–122.
18 T. Sato, V. Plashnitsa, M. Utiyama, N. Miura, *Electrochem. Commun.,* 2010, **12**, 524–526.
19 F. Liu, Y. Guan, R. Sun, X. Liang, P. Sun, F. Liu, G. Lu, *Sens. Actuators, B,* 2015, **221**, 673–680.
20 N. Miura, T. Sato, S. Anggraini, H. Ikeda, S. Zhuiykov, *Ionics*, 2014, **20**, 901–925.
21 G. Lu, Q. Diao, C. Yin, S. Yang, Y. Guan, X. Cheng, X. Liang, *Solid State Ionics*, 2014, **262**, 292–297.
22 R. Moos, K. Sahner, M. Fleischer, U. Guth, N. Barsan, U. Weimar, *Sensors*, 2009, **9**, 4323–4365.
23 Q. Diao, C. Yin, Y. Guan, X. Liang, S. Wang, Y. Liu, Y. Hu, H. Chen, G. Lu, *Sens. Actuators, B,* 2013, **177**, 397–403.
24 C. Wang, X. Cheng, X. Zhou, P. Sun, X. Hu, K. Shimanoe, G. Lu, N. Yamazoe, *ACS Appl. Mater. Interfaces*, 2014, **6**, 12031–12037.
25 H. Fan, Y. Zeng, H. Yang, X. Zheng, L. Liu, T. Zhang, *Acta Phys. Chem. Sin.,* 2008, **24**, 1292–1296.
26 P. Sun, X. Zhou, C. Wang, B. Wang, X. Xu, G. Lu, *Sens. Actuators, B,* 2014, **190**, 32–39.
27 X. Huang, Y. Jing, J. Yang, J. Ju, R. Cong, W. Gao, T. Yang, *Mater. Res. Bull.,* 2014, **51**, 271–276.
28 H. Bafrooei, E. Nassaj, T. Ebadzadeh, C. Hu, *Ceram. Int.,* 2014, **40**, 14463–14470.
29 D. Xu, H. Yang, L. Li, Q. Zhou, H. Yuan, T. Cui, *Cryst. Res. Technol.,* 2014, **49**, 502–506.
30 H. Zhang, T. Zhong, R. Sun, X. Liang, G. Lu, *RSC Adv.*, 2014, **4**, 55334–55340.
31 S. Anggraini, M. Breedon, N. Miura, *J. Electrochem. Soc.,* 2013, **160**, B164–B169.
32 L. Zhou, Q. Yuan, X. Li, J. Xu, F. Xia, J. Xiao, *Sens. Actuators, B,* 2015, **206**, 311–318.
33 G. Lu, N. Miura, N. Yamazoe, *Sens. Actuators, B,* 1996, **35-36**, 130–135.
34 N. Miura, H. Kurosawa, M. Hasei, G. Lu, N. Yamazoea, *Solid State Ionics*, 1996, **86-88**, 1069–1073.
35 N. Miura, G. Lu, N. Yamazoe, *Solid State Ionics*, 2000, **136–137**, 533–542.
36 J. Wang, P. Elumalai, D. Terada, M. Hasei, N. Miura, *Solid State Ionics*, 2006, **177**, 2305–2311.
37 P. Elumalai, J. Wang, S. Zhuiykov, D. Terada, M. Hasei, N. Miura, *J. Electrochem. Soc.*, 2005, **152**, H95–H101.
38 G. Lu, N. Miura, N. Yamazoe, *J. Mater. Chem.*, 1997, **7**, 1445–1449.
39 X. Liang, S. Yang, J. Li, H. Zhang, Q. Diao, W. Zhao, G. Lu, *Sens. Actuators, B,* 2011, **158**, 1–8.
40 P. Sun, X. Zhou, C. Wang, K. Shimanoe, G. Lu, N. Yamazoe, *J. Mater. Chem. A*, 2014, **2**, 1302–1308.
41 F. Liu, Y. Guan, R. Sun, X. Liang, P. Sun, F. Liu, G. Lu, *Sens. Actuators, B*, 2015, **221**, 673–680.
42 F. Qu, J. Liu, Y. Wang, S. Wen, Y. Chen, X. Li, S. Ruan, *Sens. Actuators, B*, 2014, **199**, 346–353.
43 M. Kasalizadeh, A. Khodadadi, Y. Mortazavi, *J. Electrochem. Soc.,* 2013, **160**, B218–B224.
44 L. Zhou, C. Li, X. Zou, J. Zhao, P. Jin, L. Feng, M. Fan, G. Li, *Sens. Actuators, B,* 2014, **197**, 370–375.
45 W. Wang, Z. Li, W. Zheng, H. Huang, C. Wang, J. Sun, *Sens. Actuators, B,* 2010, **143**, 754–758.
46 C. Feng, W. Li, C. Li, L. Zhu, H. Zhang, Y. Zhang, S. Ruan, W. Chen, L. Yu, *Sens. Actuators, B,* 2012, **166-167**, 83–88.
47 P. Sun, X. Zhou, C. Wang, K. Shimanoe, G. Lu, N. Yamazoe, *J. Mater. Chem. A,* 2014, **2**, 1302–1308.
48